ORNL/TM-2015/603

Correlation of Neutron Imaging Based Particle Image Velocimetry with Simulation of Fluid Flow Through Fractures – FY15 Summary Report

Yarom Polsky (ORNL)
Philip Bingham (ORNL)
Seth Pemberton (UTK)
Kivanc Ekici (UTK)
October 2015

OAK RIDGE NATIONAL LABORATORY
MANAGED BY UT-BATTELLE FOR THE US DEPARTMENT OF ENERGY

DOCUMENT AVAILABILITY

Reports produced after January 1, 1996, are generally available free via US Department of Energy (DOE) SciTech Connect.

Website http://www.osti.gov/scitech/

Reports produced before January 1, 1996, may be purchased by members of the public from the following source:

National Technical Information Service
5285 Port Royal Road
Springfield, VA 22161
Telephone 703-605-6000 (1-800-553-6847)
TDD 703-487-4639
Fax 703-605-6900
E-mail info@ntis.gov
Website http://www.ntis.gov/help/ordermethods.aspx

Reports are available to DOE employees, DOE contractors, Energy Technology Data Exchange representatives, and International Nuclear Information System representatives from the following source:

Office of Scientific and Technical Information
PO Box 62
Oak Ridge, TN 37831
Telephone 865-576-8401
Fax 865-576-5728
E-mail reports@osti.gov
Website http://www.osti.gov/contact.html

This report was prepared as an account of work sponsored by an agency of the United States Government. Neither the United States Government nor any agency thereof, nor any of their employees, makes any warranty, express or implied, or assumes any legal liability or responsibility for the accuracy, completeness, or usefulness of any information, apparatus, product, or process disclosed, or represents that its use would not infringe privately owned rights. Reference herein to any specific commercial product, process, or service by trade name, trademark, manufacturer, or otherwise, does not necessarily constitute or imply its endorsement, recommendation, or favoring by the United States Government or any agency thereof. The views and opinions of authors expressed herein do not necessarily state or reflect those of the United States Government or any agency thereof.

ORNL/TM-2015/603

Electrical and Electronic Systems Research Division

Correlation of Neutron Imaging Based Particle Image Velocimetry with Simulation of Fluid Flow Through Fractures – FY15 Summary Report

Yarom Polsky
Philip Bingham
Seth Pemberton
Kivanc Ekici

Date Published: *October 2015*

Prepared by
OAK RIDGE NATIONAL LABORATORY
Oak Ridge, Tennessee 37831-6283
managed by
UT-BATTELLE, LLC
for the
US DEPARTMENT OF ENERGY
under contract DE-AC05-00OR22725

CONTENTS

LIST OF FIGURES iv
LIST OF TABLES v
ABSTRACT 1
1. Background 1
2. Selection of Experimental Parameters 4
3. Summary of Results 5
   3.1 Experimental measurement of flow characeristics 5
   3.2 Simulation of experimental results 5
4. Conclusion 6
5. REFERENCES 7

LIST OF FIGURES

Figure 1 Moody Diagram 3
Figure 2 Fully developed friction factor vs. Reynolds number, both based on constricted flow hydraulic diameter; airflow. $D_{h,cf}$ = 684 μm, b = 500 μm, bcf = 354 μm, w = 10.03 mm, $\varepsilon/D_{h,cf}$ = 0.1108. (Taylor et al) 3

LIST OF TABLES

Table 1 Flow parameters for stem piece (pipe) and fracture 4

ABSTRACT

This technical memo summarizes results for evaluating the year end Go/No-Go decision for the "Application of Neutron Imaging and Scattering to Fluid Flow and Fracture in EGS Environments" project. The FY15 Go/No-Go decision criteria for the project, as written in the Annual Operating Plan, is:

Demonstrate that neutron imaging flow experiments can be used to validate flow simulation tools (either CFD or Volume of Fluids method) that can then be extended to reservoir flow models. Experiments and simulations will be performed for a simplified fracture flow scenario, flow between parallel plates, to validate technique against accepted modeling approaches.

It is claimed that this end of year decision criteria milestone was successfully met by completing a set of relevant neutron imaging experiments that measured flow through engineered fractures, with varying surface roughness, along with the development of a Volume of Fluids CFD-based simulation method that can be used to calibrate the CFD model to experimental results. This calibrated CFD-based modeling approach can then be used to calculate effective properties, in this case permeability, that can be utilized in standard reservoir flow models.

The experimental configuration, results and modeling approach are described in detail in a 2015 Stanford Geothermal Workshop paper. Rather than repeating these details, the Stanford paper is appended to this memo for reference. This memo instead adds supplemental detail explaining the rationale for selection of the experiments performed and their relevance to modeling and simulation approaches related to reservoir monitoring. A high level summary of the research results and description of the methodology for utilizing experimental results in a modeling framework is also provided in this memo.

1. Background

Extensive work has been performed over the years by many researchers to determine an appropriate computational model for flow in fractures (representative work is cited in the References section of this document). Reservoir scale simulators typically use simplified models of flow, such as Darcy flow, given as

$$Q = -\frac{k}{\mu}\nabla p$$

where Q is the flow rate, k is the permeability, ∇p is the pressure gradient, and μ is the viscosity of the fluid. The Darcy model is used to predict flow rate or pressure drop through a fracture network.

Natural fractures tend to have geometric complexities, such as surface roughness, larger scale asperity variation, and variation in fracture trajectory such as tortuosity. These naturally present features will affect mean velocities through the fracture and must be accounted for in the reservoir simulator by using effective or average values for permeability. They can also create the possibility that the flow will transition to a turbulent regime. If the transition occurs, then the measurable quantities like pressure drop and /or flow rate could be affected significantly.

The experiments undertaken this FY were intended to demonstrate that flow behavior in situations where deviations from idealized model geometries occur can be quantified using neutron imaging. This research then shows that these measurements can be used as a basis for calibrating more comprehensive modeling approaches, such as computational fluid dynamics, that are too computationally expensive to implement on a reservoir scale, but can be used as a tool to calculate fluid parameters for reduced order models used in reservoir scale simulators. The remainder of this section will describe the basis for simple experimental demonstrations that can validate this approach.

While arbitrary aperture variation of the fracture faces can be accommodated in our experimental configuration, it was decided that initial experiments would focus on simple sample configurations to facilitate systematic development of modeling approaches. Flow between nominally parallel surfaces represents the simplest experimental scenario. This geometry is easy to model and can be more easily correlated to simulation results and studies in the literature.

Generally, it is assumed that flow in fractures is of low Reynolds number and thus laminar. Since flow regimes are a function of Reynolds number (*Re*), target Reynolds numbers were defined for experimental measurement in the laminar to turbulent transition region. The Reynolds number is defined as

$$Re = \frac{\rho U b}{\mu}$$

where ρ is the density, U is the average velocity, and b is the aperture size. In our experiments, the desired Re was achieved by controlling the in flow rate (velocity). From the literature, it is well-known that transition to turbulence in channels begins for Reynolds numbers anywhere between1100 to 1400, depending on inlet conditions. Fully turbulent flow is expected at 2400.

In addition to measuring flow behavior near the transition region, the current research also introduced order variation in the form of surface finish to demonstrate the ability of the developed experimental technique to measure the associated flow variation. This represents a relatively simple departure from the idealized nominally flat plate geometry. Surface roughness is generally characterized by the average roughness over the entire surface of a material. Recently, there has been research focused on describing roughness with characteristics in addition to average roughness, especially for mini-channels and micro-channels. For the purposes of the proof-of-concept experiments undertaken, producing in-depth roughness features in samples was avoided in order to simplify the modeling component of this research. Therefore, the Moody diagram was used as a starting point for specifying roughness values that would produce transition flow for particular flow rates.

It is emphasized that the goal of the current study is not to simulate transition flow. Transition flow is very difficult to model and simulate. The desire to produce varying flow regimes for identical aperture sizes in this study is to demonstrate that baseline flow in the laminar regime can be simulated using a relevant CFD approach while also demonstrating that the developed experimental setup can be used to quantify departures from the baseline case. An experimental data set with flow field detail can then be used to support the development of simulation tools that incorporate transition behaviors and fine tune modeling parameters.

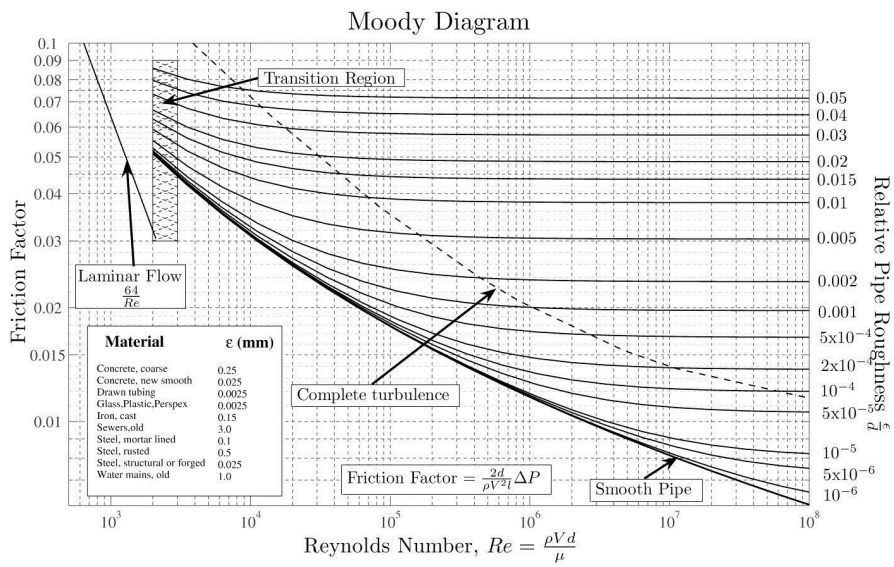

Figure1. Moody Diagram

Based on the Moody diagram given in Figure 1, relative roughness values of ~0, 0.015 and 0.05 were chosen for experimental purposes. These selections correspond to low, intermediate and high levels of roughness on the Moody Diagram with significantly different turbulent Re number regimes. Other researchers have examined the effects of surface roughness on transition flow (a good summary is presented in Taylor et al). The experimental results provided in Figure 2 below are for a rough channel and show a transition from laminar to turbulent flow beginning at a Reynolds number of approximately 600. Target experimental flow rates corresponding to Re numbers between 600 and 2000 were therefore examined based on the current capabilities of the neutron imaging setup. As mentioned earlier, it was expected that flow in this range would permit the validation of laminar flow models as well as the experimental demonstration of deviations from laminar behavior to affirm the basis of the experimental method as a means of quantifying flow behavior.

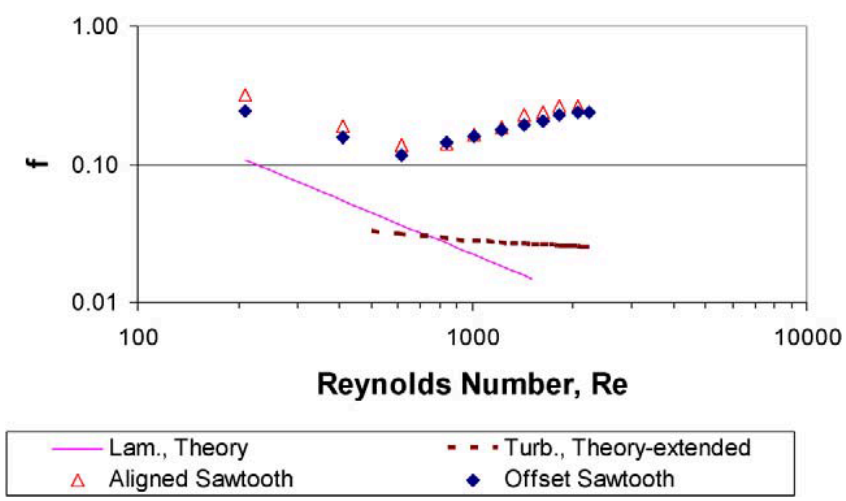

Figure 2. Fully developed friction factor vs. Reynolds number, both based on constricted flow hydraulic diameter; airflow. Dh,cf = 684 µm, b = 500 µm, bcf = 354 µm, w = 10.03 mm, ε/Dh,cf = 0.1108. (Taylor et al)

2. Selection of Experimental Parameters

There are two distinct flow geometries associated with the experimental configuration: the flow inlet to the pressure cell through the stem piece and the flow through the sample fracture. The former is a pipe geometry while the latter is a channel geometry. For additional explanation on the stem piece used, we refer the reader to Appendix A, our Stanford Workshop paper. The table presented below shows calculated Reynolds numbers for the two geometries. The pipe Reynolds number reaches the critical Re at a lower system volumetric flow rate than the channel Re because the hydraulic diameter of the channel section is considerably larger. In fact, the Pipe Re is four times that of the channel Re at the same flow rate. Because the flow in the channel section arrives from the pipe inlet, this creates some uncertainty regarding whether or not the entrance flow in the channel will be turbulent. There is a transition section in the stem piece designed to gradually adjust the flow characteristics to match the two geometries, but there is a limited length over which this occurs due to practical limitation of the pressure cell size. An experimental flow rate between 0.7 lpm and 1 lpm was therefore selected to produce flow in the expected transition region. It is also pointed out that the flow velocities corresponding to this flow rate are at the upper limit of the current capabilities of the neutron imaging beam line utilized for the experiments.

Table 1. Flow parameters for stem piece (pipe) and fracture

Density [kg/m^3]	Diameter [m]	Pipe Area [m^2]	Frac. Perimeter [m]	Frac. Area [m^2]	Frac. Hyd. Dia. [m]	nu [m^2/s]	Aperture b [m]
1000	0.00635	0.00003167	0.079375	6.05E-05	0.00305	9.78E-07	0.0015875

Flow Rate [L/min]	Pipe Avg. Vel. [m/s]	Frac. Avg. Vel. [m/s]	Pipe Re	Frac. Re	ε/D_h	ε [m]	ε/b
0.1	0.0526	0.0276	341.7	85.9	0	0	0
0.2	0.1053	0.0551	683.4	171.8	0.015	4.57E-05	0.0288
0.3	0.1579	0.0827	1025.1	257.6	0.05	0.000152	0.096
0.4	0.2105	0.1102	1366.7	343.5			
0.5	0.2631	0.1378	1708.4	429.4			
0.6	0.3158	0.1653	2050.1	515.3			
0.7	0.3684	0.1929	2391.8	601.1			
0.8	0.4210	0.2204	2733.5	687.0			
0.9	0.4736	0.2480	3075.2	772.9			
1.0	0.5263	0.2755	3416.9	858.8			
1.1	0.5789	0.3031	3758.6	944.6			
1.2	0.6315	0.3307	4100.2	1030.5			
1.4	0.7368	0.3858	4783.6	1202.3			
1.6	0.8420	0.4409	5467.0	1374.0			
1.8	0.9473	0.4960	6150.4	1545.8			
2.0	1.0525	0.5511	6833.7	1717.5			

ε is the roughness height

3. Summary of Results

As stated earlier in this memo, most of the technical detail related to this work is covered in the Stanford paper in Appendix A. This includes: the experimental setup, neutron imaging considerations, particle image velocimetry approach, Volume of Fluids model description, experimental results and comparison of simulation and experimental results. This section will provide a concise summary of the results as they related to the end of year Go/No-Go decision milestone for the project. This summary highlights the following aspects of the work performed as they relate to the project goal: 1) The ability of the developed experimental method to measure flow characteristics relevant to flow through fractures, and 2) The use of an advanced computational modeling capability to simulate experimental results for future correlation to reduced-order model parameters.

3.1 EXPERIMENTAL MEASUREMENT OF FLOW CHARACERISTICS

The velocimetry measurements given in Fig. 6 of the Stanford paper clearly demonstrate the ability of the developed technique to quantitatively measure both local flow velocity and direction. As stated in the Stanford paper, because the contrast agent has fluid properties that are slightly different from water (e.g. specific gravity and viscosity), simulation must be used to correlate the behavior of the tracked bubbles to the local flow field. This modeling correlation was successfully demonstrated as will be discussed in the next section. It is also pointed out that the experimental setup has undergone significant refinement this FY with the development of a needle bubbler injection section that facilitates significantly more controlled introduction of contrast agent into the flow stream. This controlled injection minimizes the disturbance of the bulk flow field. Future efforts by this group or others can continue to refine the particle seeding of the flow by identifying liquid contrast agents more closely matched to bulk fluid properties or perhaps developing engineered particles of solid form.

The other indication of the value of this experimental method for understanding and measuring flow through non-idealized fracture geometries can be seen in Table 1 of the Stanford paper. This imaging based measurement method generates a large volume of data related to the flow field. The statistics of the measurements provide useful insight into the dominating flow mechanisms. In the case of the 0.825 lpm flow data, for example, the standard deviation of the particle velocities was considerably higher for both rough samples versus the smooth samples. This likely indicates behavior more representative of flow in the laminar to turbulent transition regime as is expected with the earlier onset of this condition for higher surface roughness levels.

3.2 SIMULATION OF EXPERIMENTAL RESULTS

The success of simulation efforts to represent flow effects is best seen in Figs. 8 and 9 of the Stanford paper. The simulated droplet velocities in Fig. 8, in particular, very closely match the measured values for the 0.825 lpm volumetric flow rate for the smooth sample in Table 1. This is considered to be a reasonable validation that the correlation of simulation to experimental results is feasible. Figure 8 of the Stanford paper also highlights the importance of this correlation because the simulated velocity of the centerline velocity without contrast agent is considerably higher than the droplet velocity. Similarly, the image views of the contrast agent droplet shape for the simulation and the neutron radiograph are reasonably well matched.

4. CONCLUSION

The work performed in FY 15 was able to successfully demonstrate that particle image velocimetry of flow through fractures in a pressure cell using neutron radiography can produce sufficient flow structure detail to be correlated to Navier-Stokes based computational fluid models. While further refinement of the experimental configuration is recommended, the current setup is able to produce flow field measurements of experiments relevant to understanding and predicting flow through fractured media. Volume of Fluids simulations of experimental conditions were also performed with good correspondence between simulated flow values and measured flow values. These results collectively validate a viable pathway to utilize the developed experimental method to directly determine effective property values for reduced-order models or to calibrate Navier-Stokes based computational fluid models for use as a tool to determine effective property values for reduced-order models that can be applied to reservoir scales.

5. REFERENCES

Bertels, S. P., DiCarlo, D. A., & Blunt, M. J. (2001, March). Measurement of aperture distribution, capillary pressure, relative permeability, and in situ saturation in a rock fracture using computed tomography scanning. *Water Resources Research, 37*(3), 649-662.

Boussinesq, J. (1868). Memoire sur I'influence des frottements dans les movements reguliers des fluides. *Journal of Math. Pure Appl., 2*(13), 377-424.

Brown, S. R. (1987, Feburary). Fluid Flow Through Rock Joints: The Effect of Surface Roughness. *Journal of Geophysical Research, 92*(B2), 1337-1347.

Brown, S. R., & Scholz, C. H. (1985b). Broad badwidth study of the topography of natural rock surfaces. *Journal of Geophysical Research, 90*, 12575-12582.

Brown, S. R., Stockman, H. W., & Reeves, S. J. (1995, September). Applicability of the Reynolds-equation for modeling fluid flow between rough surfaces. *Geophysical Research Letters, 22*(18), 2537-2540.

Brush, D. J., & Thomson, N. R. (2003). Fluid flow in synthetic rough-walled fractures: Navier-Stokes, Stokes, and local cubic law simulations. *Water Resources Research, 39*(4), 1085.
Cardenas, M. B., Slottke, D. T., Ketcham, R. A., & Sharp Jr., J. M. (2009). Effects of inertia and directionality on flow and transport in a rough asymmetric fracture. *Journal of Geophysical Research, 114*.

Crandall, D., Ahmadi, G., & Smith, D. H. (2010). Computational Modeling of Fluid Flow through a Fracture in Permeable Rock. *Transport in Porous Media, 84*, 493-510.
de Marsily, G. (1986). *Quantitative Hydrogeology.* San Diego, California: Aca
demic Press.
Dicman, A., Putra, E., & Schechter, D. A. (2004). Modeling Fluid Flow Through Single Fracture Using Experimental, Stochastic and Simulation Approches. *SPE/DOE Fourteenth Symposium on Improved Oil Recovery.* Tulsa, Oklahoma: Society of Petroleum Engineers.

Dijk, P., Berkowitz, B., & Bendel, P. (1999, Feburary). Investigation of flow in water-saturated rock fractures using nuclear magnetic resonnace imaging (NMRI). *Water Resources Research, 35*(2), 347-360.

Fournier, A., Fussel, D., & Carpenter, L. (1982). Computer rendering of stochastic models. *Communications of the Associated Computing Machinery, 25*(6), 371-384.
Hirono, T., Takahashi, M., & Nakashima, S. (2003). In situ visualization of fluid flow image within deforme rock by X-ray CT. *Engineering Geology, 70*, 37-46.

Karpyn, Z. T., Grader, A. S., & Hallek, P. M. (2007). Visualization of fluid occupancy in a rough fracture using micro-tomography. *Journal of Colloid and Interface Science, 307*, 181-187.
Keller, A. (1998). High Resolution, Non-destructive Measurement and Charaterization of Fracture Apertures. *International Journal of Rock Mechanics and Mining Science, 35*(8), 1037-

1050.

Klimczak, C., Schultz, R. A., Parashar, R., & Reeves, D. M. (2010, Feburary). Cubic law with aperture-length correlation: implications for network scale fluid flow. *Hydrogeology Journal*.
Lavrov, A. (2013). Numerical modeling of stead-state flow of a non-Newtonian power-law fluid in a rough-walled fracture. *Computers and Geotechnics, 50*, 101-109.

Liu, Q., & Fan, H. (2012). The characteristics and estimation of flow through a single rough-walled fracture. *Journal of Hydrodynamics, 24*(3), 315-322.

Lomize, G. (1951). *Flow in Fractured Rocks.* Moscow: Gosenergoizdat.
Louis, C. (1969). A Study of Groundwater Flow in Jointed Rock and Its Influences on the Stability of Rock Masses. *Rock Mechanics Research Report*(10), 90.

Neuzil, C. E., & Tracy, J. V. (1981, Feburary). Flow Through Fracture. *Water Resorces Research, 17*(1), 191-199.

O'Sullivan, M. J., Pruess, K., & Lippmann, M. J. (2001). State of the art of geothermal reservoir simulation. *Geothermics, 30*, 395-429.

Radilla, G., Nowamooz, A., & Fourar, M. (2013). Modeling Non-Darcian Single and Two-Phase Flow in Transparent Replicas of Rough-Walled Fracture. *Transport in Porous Media, 98*, 401-426.

Snow, D. (1965). *A paralell plate model of fractured permeable media.* Ph.D. thesis, University of California, Berkeley.

Taylor, J.B., Andres, L.C., and Kandilkar, S.G., "Characterization of effect of surface roughness and texture on fluid flow –past, present, and future", *Int. J. of Thermal Science*, Vol. 45. Pp. 962-968, 2006.

Tsang, Y. W. (1984). The Effect of Tortuosity on Fluid-Flow Through a Single Fracture. *Water Resources Research, 20*(9), 1209-1215.

Waite, M. E., Ge, S., & Hartmut, S. (1999, June). A new conceptual model for fluid flow in discrete fractures: An experimental and numerical study. *Journal of Geophysical Research, 104*(B6), 13049-13059.

Walsh, J. B. (1981). Effect of pore pressure and confining pressure on fracture permeability. *International Journal of Rock Mechanics and Mining Sciences, 18*(5), 429-435.

Witherspoon, P. A., Wang, J. S., Iwai, K., & Gale, J. E. (1980, December). Validity of Cubic Law for Fluid Flow in a Deformable Rock Fracture. *Water Resources Research, 16*(6), 1016-1024.

Zhang, Z., & Nemcik, J. (2013). Fluid flow regimes and nonlinear flow characteristics in deformable rock fractures. *Journal of Hydrology, 477*, 139-151.

Zimmerman, R. W. (1996). Hydraulic Conductivity of Rock Fractures. *Transport in Porous Media, 23*, 1-30.

APPENDIX A. 2015 Stanford Geothermal Workshop Paper

PROCEEDINGS, Fourtieth Workshop on Geothermal Reservoir Engineering
Stanford University, Stanford, California, January 26-28, 2015
SGP-TR-204

Particle Imaging Velocimetry Technique Development for Laboratory Measurement of Fracture Flow Inside a Pressure Vessel Using Neutron Imaging

Yarom Polsky[1], Philip Bingham[1], Hassina Bilheux[1], Justin Carmichael[1], Seth Pemberton[2], Kivanc Ekici[2], Daniel S. Hussey[3] and David Jacobson[3]

[1]*Oak Ridge National Laboratory, Oak Ridge, TN 37831 USA*
[2]*University of Tennessee, Knoxville, TN 37996 USA*
[3] *National Institute of Standards and Technology, Gaithersburg, MD 20899 USA*

Email: polskyy@ornl.gov

Keywords: Flow measurement, flow simulation, fractures, EGS, imaging, experimental methods

ABSTRACT

This paper will describe recent progress made in developing neutron imaging based particle imaging velocimetry techniques for visualizing and quantifying flow structure through a high pressure flow cell with high temperature capability (up to 350 °C). This experimental capability has great potential for improving the understanding of flow through fractured systems in applications such as enhanced geothermal systems (EGS). For example, flow structure measurement can be used to develop and validate single phase flow models used for simulation, experimentally identify critical transition regions and their dependence on fracture features such as surface roughness, and study multiphase fluid behavior within fractured systems. The developed method involves the controlled injection of a high contrast fluid into a water flow stream to produce droplets that can be tracked using neutron radiography. A description of the experimental setup will be provided along with an overview of the algorithms used to automatically track droplets and relate them to the velocity gradient in the flow stream. Experimental results will be reported along with Volume of Fluids based simulation techniques used to model observed flow.

1. INTRODUCTION

Characterizing and modeling flow in porous and fractured media has been a topic of active and intense research in subsurface hydrology and, later, reservoir engineering since Henry Darcy first formulated his phenomenological law describing flow through permeable media in 1856. The importance of understanding subsurface flow processes has increased dramatically since Darcy's time as we have come to rely on the subsurface as our primary source of energy, an increasingly important source of water, and the preferred disposal location for hazardous wastes. The models used to describe flow through porous and fractured media have become the basis for reservoir scale simulators that are used as decision making tools in a number of reservoir engineering applications including, but not limited to: evaluating reservoir development strategies (e.g. well placement, well trajectory, completion design, etc.), long-term well field performance and economic analysis, production management and enhanced recovery. The commercial demonstration of Enhanced Geothermal Systems (EGS) will be especially reliant on the use of such reservoir simulation tools to explore potential well field designs and production scenarios because of the limited field experience associated with non-hydrothermal geothermal systems. However, the underlying models of fracture flow in conventional reservoir simulators are numerical simplifications with a tenuous relationship to the actual physical characteristics of real fractures.

Simplified or alternatively, reduced-order models are used as the basis for large scale simulations because of the large computational expense associated with higher fidelity approaches such as Navier-Stokes formulations. A reasonable review of approaches used to characterize fracture flow is presented by [Berkowitz (2002)]. The idealized model of a smooth fracture based on Poisueille flow through parallel plates, more commonly referred to as the cubic law, has been validated in the laboratory for open fractures, including tensile fractures in geological specimens under laminar conditions [Witherspoon (1980)]. Numerous corrections have been proposed to the cubic law to account for geometric variation of the fracture such as roughness and tortuosity [Neuzil (1980), Waite (1999), Klimczack (2010)].

Some experimental efforts have focused on creating carefully constructed fracture geometries, for which surface roughness and aperture variation can be quantified, and measuring flow rates through the fracture to develop modified cubic laws [Hakami (1996), Qian (210)]. The effects of tortuosity on fluid flow has been investigated using optical imaging methods [Rush (1999)]. More recent experimental investigations have attempted to relate roughness and other surface effects, such as wettability, to multiphase flow through fractures using optical imaging techniques for which fluids of interest flow between one half of a real fractured rock and a transparent casting of the opposing fracture piece [Babadagali (2015)].

This paper describes ongoing efforts to develop a novel method for visualizing and quantifying flow structure in fractured geological media. The developed method involves the controlled injection of a high contrast fluid into a water flow stream to produce droplets that can be tracked using neutron radiography. This method is intended to be used to validate reduced-order models of flow through fractures. A description of the experimental setup will be provided along with an overview of the algorithms used to automatically track

droplets and relate them to the velocity gradient in the flow stream. Experimental results will be reported along with preliminary Volume of Fluids method simulation techniques used to model observed flow.

2. EXPERIMENTAL SETUP

2.1 Overview

The approach utilized in this work follows standard particle imaging flow measurement techniques. These techniques are conventionally employed using optical or laser-based methods and have also been applied using nuclear magnetic resonance methods [Adrian (1991)]. The use of neutron radiography to measure contrast agents in forced aqueous flow fields, through fractures in particular, is believed to be unique. Neutron radiography (imaging) has an advantage over conventional optical methods because it can be utilized when flow-bounding materials such as rock and pressure vessel walls are opaque.

Multiple contrast agents have been explored in this research including miscible fluids, immiscible fluids, and solid particles. For all types, the locations of the entrained particle bunches or droplets are measured in successive images to compute their Lagrangian velocity. Since we are ultimately interested in measuring the Eulerian flow field of the system, some consideration must be given to both the ability of the particle or droplet to accurately follow the flow movement as well as any perturbing effect it might have on the flow field. Good correspondence between the measured Lagrangian velocity vectors and the Eulerian flow field is typically achieved by matching the properties of the tracked material to the fluid properties as closely as possible. The measured material must also have a significantly different neutron scattering contrast as compared to water in order to be discernible in the acquired radiographs.

Earlier work associated with this research utilized slugs of heavy water (D_2O) as a tracked object because of its high contrast with water and good matching of properties. D_2O has approximately 1/9 the total scattering cross section for thermal neutrons of H_2O, identical viscosity, and 11% greater density. These efforts were unable to produce images that could be converted to useful velocity maps of the flow field because the introduction of the contrast slugs occurred far upstream of the inlet to the pressure cell and the miscibility of the two fluids resulted in significant dilution of the D_2O before entering the fracture. The presence of the diluted mixture could be observed on average over large regions of the image, but fine detail of the mixture flow front was not measurable as the front progressed across the image view. An example of this difficulty is presented in figure 1 below. The figure shows sequential images of flow through an engineered granite fracture with a width of 31.75 mm and aperture of 1.6 mm. The graph in the upper right of the figure shows the average attenuation versus image capture frame for a small area region within each captured image (region shown in upper left of graph). The absence of a sharp intensity transition as the slug enters the monitoring window is indicative of significant dilution of the contrast slug. Additional efforts to seed water flow with solid particles, such as silica and polyethylene beads, with diameter ranging from 100 μm – 300 μm, produced similar results. In these cases, individual particles could not be identified within the flow field and particle grouping was generally poor resulting in a lack of objects that could be tracked and correlated to the flow field.

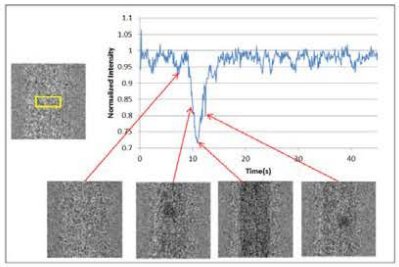

Figure 1. Normalized intensity within a control volume for D_2O injected into an H_2O flow stream.

More recent experiments have focused on the use of immiscible fluids as tracked objects. These experiments have been carried out with Fluorinert™*, a perfluorinated liquid typically used to mitigate breakdown in high voltage electronic applications or as a cooling medium in electronic applications. Fluorinert™ has a neutron scattering cross section of approximately 5 % that of water and can be introduced in a controlled manner with consistent droplet sizes into the flow field as will be discussed in a subsequent section. Promising results have been obtained to date as will be shown in later sections. The properties of Fluorinert™ are not matched to H_2O. It has a density of 1820 kg/m^3 and absolute viscosity of 1.4 centipoise. This does present some challenges with respect to determining the Eulerian flow field as the droplet fluid velocity tends to lag that of the flow field. Navier-Stokes based computational fluid dynamic methods are used to simulate and match the measured flow field in order to relate average velocities to a reduced-order model or representation of the flow.

* Certain trade names and company products are mentioned in the text or identified in an illustration in order to adequately specify the experimental procedure and equipment used. In no case does such identification imply recommendation or endorsement by the National Institute of Standards and Technology, nor does it imply that the products are necessarily the best available for the purpose.

2.2 Hardware Description

The experimental method utilizes a pressure cell that has been developed for neutron experiments (figure 2). It holds a cylindrical specimen with a diameter of 38.1 mm, length of up to 152.4 mm and is capable of applying independent radial and axial confining pressures to the sample. Flow enters and exits the sample in the axial direction through fluid ports at opposite ends of the pressure cell (item 2 in figure 2). Details of the pressure cell and flow system design are described in [Polsky et al (2013)]. This publication will describe improvements to the system since earlier reported work.

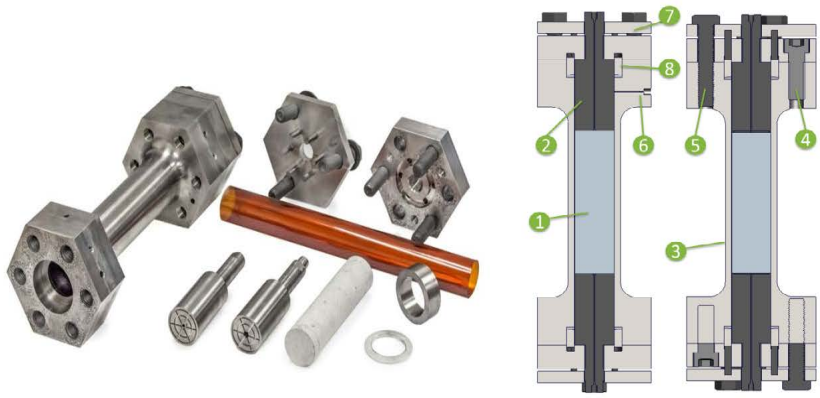

Figure 2. Chamber design (left) Picture of separated components (right) schematic (1) test specimen (2) flow entrance (or exit) piece (3) vessel body (4) internal retaining fasteners (5) seal forming fasteners (6) liner pressure port (7) seal forming plate assembly (8) seal area

There have been three major hardware improvements to the fluid flow imaging capabilities of the system since initial experiments: the use of an Aluminum body instead of a Titanium body for lower temperature experiments; redesign of the flow entrance and exit ports; and the addition of a needle bubbler system to introduce liquid contrast agents that can be tracked to quantify flow structure.

2.2.1 Pressure Cell Material Selection

The use of Aluminum as a material for the pressure cell was introduced in order to decrease the attenuation of the neutron beam due to its passage through the cell. The combined absorption and incoherent scattering cross sections for Titanium are approximately 31.25 times larger than that of Aluminum for the 1.8 angstrom thermal neutrons used at the NIST imaging beam line [Jacobson (2006)]. Calculated transmission through 1 cm of Aluminum, approximately twice the thickness of the pressure cell wall, is 98.5 %. Transmission through a comparable thickness of Titanium is only 60.7%. There is therefore a significant improvement in the transmitted neutron flux through a cell composed of Aluminum, although the maximum operating temperature of the cell becomes de-rated to 200 °C for high pressure testing with this material.

This increased neutron fluence rate becomes important for high flow rate experiments because the image exposure time must be reduced if individual particle tracking is desired. The most observable contrast agents we have thus far attempted require minimum exposure times of between 10 ms and 20 ms in order to distinguish them in the aqueous flow field. A particle with a velocity of 30 cm/s will move between 3 mm and 6 mm in this time window resulting in a significant blurring of the droplet when its diameter is on the same dimensional order. If the image field of view is small, as is the case when smaller area imagers such as multi-channel plate neutron detectors are used, then additional consideration must be given to the smaller number of frames that will be captured showing the particle as it moves across the field of view. This reduced number of captured frames produced fewer particle velocity vectors making it difficult to ascertain the fluid flow field. It is therefore desirable to maximize flux for high flow rate experiments.

2.2.2 Fluid Flow Inlet and Exit Redesign

The initial system configuration utilized a flow inlet with a single circular channel, as shown below in figure 3a, with the single channel directly impinging on the surface of the sample. It is noted that the geometry of this interface is such that the diameter of the circular inlet channel is generally substantially larger than the aperture of the fracture. This configuration is not ideal for particle or droplet injection experiments for a number of reasons. First, many of the particles leaving the circular channel impact the sample face prior to entering the rectangular fracture. Second, this arrangement produces a "jetting" effect at the center of the sample when the sample contains a fracture with a rectangular geometry. This jetting effect produces large axial velocity gradients in the transverse direction at

the entrance to the fracture and also produces transverse fluid velocities that would not normally be expected for fully developed flow conditions within the fracture.

To mitigate these effects, a funnel-type transition from a circular to rectangular cross section is incorporated into the new flow inlet piece. There is approximately 14 cm of rectangular cross section following the circular to rectangular transition to allow the flow profile to normalize prior to entering the sample. The improved design is shown in figure 3b. A removable aperture matching section was also incorporated in the design to allow additional adjustment of the flow stem aperture to more closely match the sample aperture.

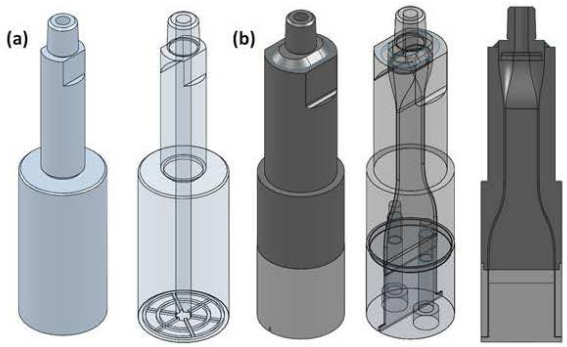

Figure 3: Solid and transparent views of (a) original fluid flow stem, and (b) modified fluid flow stem.

Computational fluid dynamic simulations of the flow field within the flow stem and a representative fracture with an aperture of 1.6 mm are shown in figure 4. These results were obtained using the COMSOL Multiphysics 4.4 software. The contour plots to the left of the figure show axial flow velocities on a plane parallel to the fracture faces at the center of the aperture. Note that the flow direction is from right to left in these simulations. The line plots to the right of the figure show the axial velocity as a position of height within the fracture at axial positions of 0 mm (the entrance to the fracture), 25 mm and 50 mm. The jetting effect at the center of the fracture is clearly visible for the original design. As can be seen in figure 4b, the velocity gradients for the new design are substantially lower by comparison. It is further pointed out that the transverse velocity gradient at the inlet of the new design is roughly 10% that of the original design.

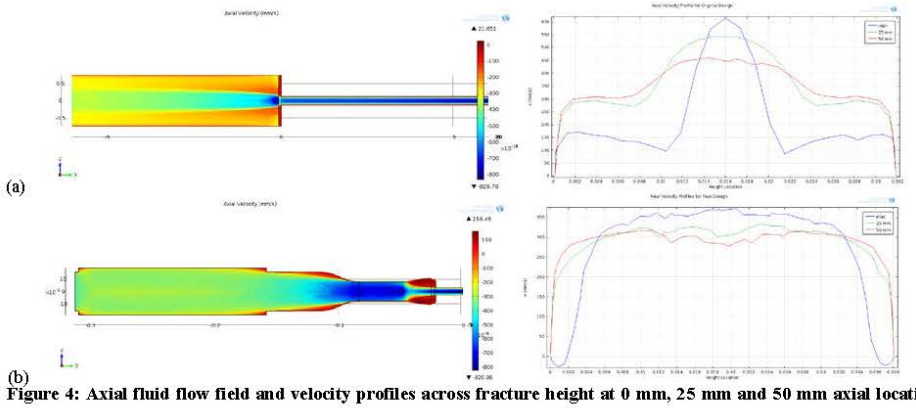

Figure 4: Axial fluid flow field and velocity profiles across fracture height at 0 mm, 25 mm and 50 mm axial location for (a) original flow stem and (b) new flow stem designs.

2.2.3 Contrast Slug Injection

Injection of the contrast agent into the flow stream was initially performed at the primary fluid pump suction inlet. This method resulted in significant mixing of contrast liquid with the aqueous fluid stream. A subsequent implementation introduced a parallel circuit in the high pressure discharge line coming from the pump. A volume of contrast agent could be placed in the parallel circuit prior to pumping and could introduced into the primary flow stream by diverting flow through the section using a two position valve during pumping. This was an improvement to the original system but produced droplets of variable size, most of which were excessively large, resulting in disturbance of the aqueous flow field. The current version of the flow system utilizes a high pressure syringe style pump with a needle bubbler as shown in figure 5 below. The needle bubbler is made with 1.5875 mm (1/16") HIP high pressure tubing with a 0.15 mm inner diameter that is inserted midway into the primary fluid line through a tee. The injection rate of the pump can be controlled to flow rates ranging between 0.01 mL/min up to 30 mL/min to meter in small volumes of contrast agent. This configuration is able to produce small droplets with reproducible size and frequency and has proven to produce good results.

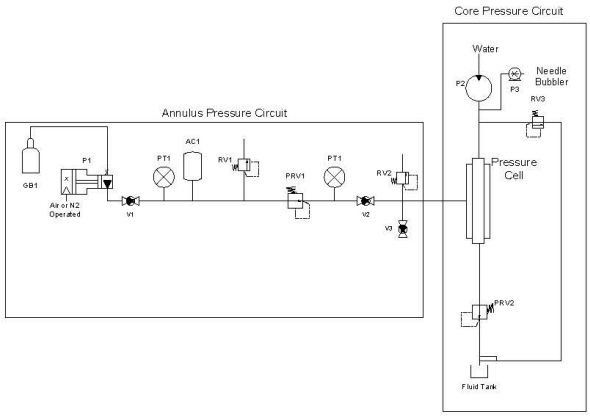

Figure 5: Pressure cell flow schematic

3. EXPERIMENTAL RESULTS

3.1 Image processing and tracking algorithm

The objective of the image processing algorithm is to automatically identify and track the path of each droplet in the captured image sequence. The developed algorithm consists of two major subroutines: a segmentation routine and a tracking routine. Normalization of the images is first performed following a typical radiographic processing method where a dark image is subtracted, the result is divided by an open beam, and the natural log is taken. For this effort, the open beam is replaced by an image containing no droplets such that the water, rock, and chamber are removed resulting in a difference image containing only the droplets. Next, a threshold is performed to create a binary image of the droplets. Voids are removed from the segments and the edges are smoothed with a dilation operation. The results of the segmentation algorithm is a table containing the (x,y) location of the centroid, the area, and the image number for each droplet segmented in the image series.

Particle image velocimetry processing will typically use correlation algorithms to track the location of segments from frame to frame. Since the image stacks for this application contain clusters of droplets where the droplets move independently and the droplets move farther between image frames than the distance between droplets in the frames, correlation algorithms do not work well in this case. Therefore, a rules based tracking algorithm based on probabilities is used. Additional challenges for the algorithm are droplet sticking, joining, and splitting.

In a frame by frame fashion, the tracking algorithm first calculates the velocity vector between each segmented droplet and all of the droplets in the previous frame. A probability distribution function based on the velocity vector is used to select the most probable link between droplets. A binomial function is used to account for moving and stuck droplets. The moving droplets portion of the function is a Gaussian distribution with a standard deviation with a mean equal to the distance moved by the droplet in the previous step and a standard deviation equal to a 10 pixel shift. For a new droplet that has yet to be tracked, an initial velocity is set by the user for the mean. Since the tracking portion of the algorithm is fast, the user can iterate on this initial velocity threshold to obtain the best results. Stuck droplets are represented in the probability by a Gaussian distribution centered at 0 pixel shift and a 10 pixel shift standard deviation. The moving and still distributions are combined with a weighted sum with weights of 0.9 and 0.1 respectively. In these

measurements, droplets are not able to move against the flow, so the probability function is set to zero for droplets moving in opposite direction. After iterating through all droplets, tracks for any previous droplets that are not assigned to the new frame are stopped, and any droplets in the new frame that are not linked to previous tracks are labeled as new tracks. With this method, if a droplet is not detected in each frame, it will result in multiple shorter tracks. As a result, longer tracks represent more reliable droplet detections. To prevent jumping of tracks a rule was implemented in the track algorithm that the distance along the direction of flow must be more than two times greater than the perpendicular direction.

3.1 Results

Experiments were performed using an immiscible contrast agent, Fluorinert™, injected into the aqueous flow field for variable flow rates through an engineered fracture created by offsetting split cylindrical sections of aluminum. The aluminum surfaces were machined with either a smooth finish, medium rough finish or rough finish. The average roughness values were not quantified. All samples had a height of 31.75 mm and length of 152.4 mm. Smooth finished sections had an aperture of 1.5 mm while rough finished sections had an aperture of 0.75 mm. Smaller spacer shims were used for the rough samples because they were dimensionally out of tolerance and would not fit in the pressure cell with the 1.5 mm spacer shims.

It is noted that these results were obtained using the parallel circuit injection technique, instead of the needle bubbling technique described in section 2.2.3. The needle bubbling configuration has been implemented at a neutron imaging beam line, but the beam line was not optimally configured at the time and image quality was poor due to reduced neutron fluxes. The acquired neutron radiographs could be evaluated and compared using the human eye, and appear to produce improved results, but the droplet contrast was too low for the automated tracking algorithm to map its velocity. Experiments using the needle bubbler configuration with an optimized neutron instrument configuration are planned for a later date. It is also noted that the parallel circuit injection technique produces very large droplets that are susceptible to disaggregation and joining. The droplets produced in this manner are neither controlled nor optimal because they are more prone to sticking to the fracture walls and/or distorting the flow field.

The images to the left in figure 6 shows velocity vectors computed by the tracking algorithm for different experimental parameters, while the images on the right show representative radiographs captured for that flow experiment. The flow trajectories are generally linear, indicating that flow is laminar, with increasing velocity change with pump flow rate. Average and median velocities, along with the standard deviations, for each flow experiment are presented in table1. The quantitative relationships between the flow field and the experimental parameters should be viewed cautiously for these experiments because actual flow rates were estimated based on pump rpm as opposed to measured directly. More complete data sets will be gathered in future experiments. The general trends in the data are nonetheless reasonable and the develop vector plots of the droplet velocities demonstrate the potential usefulness of this experimental method.

Table 1: Average velocity, median velocity and standard deviation for flow experiments

Sample Description	Aperture	Vavg (mm/s)	Vmedian (mm/s)	STDEV (mm/s)
0.65 lpm smooth	1.5 mm	147.9	156.09	35.34
0.825 lpm smooth	1.5 mm	196.11	196.23	21.51
1 lpm smooth	1.5 mm	210.3	211.5	29.1
0.825 lpm medium	0.75 mm	292.02	294	55.35
0.825 lpm rough	0.75 mm	273.99	284.46	63.9

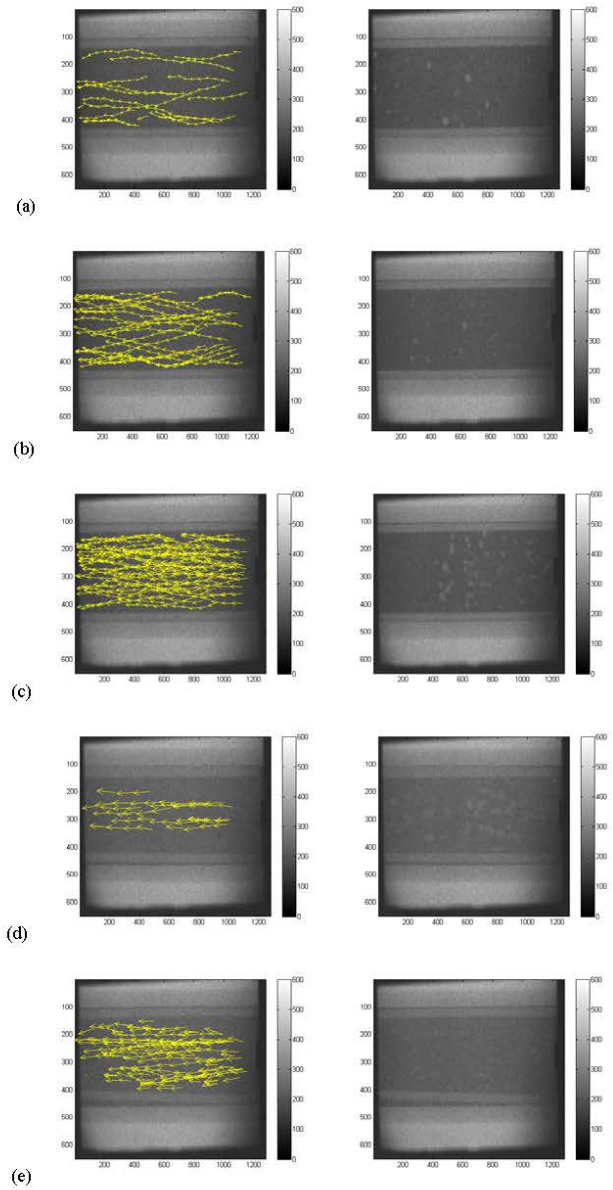

Figure 6: Velocity vectors and representative radiographs from (a) 0.65 l/min smooth aluminum fracture, (b) 0.825 l/min smooth aluminum fracture, (c) 0.825 l/min medium rough aluminum fracture, (d) 0.825 l/min rough aluminum fracture and (e) 1 l/min smooth aluminum fracture flow experiments

5. SIMULATION RESULTS

5.1 Simulation Overview

Simulation of experimental results was performed with the Volume of Fluid (VOF) method using the open-source OpenFOAM software. The governing equations for two isothermal, incompressible, immiscible fluids include the continuity, momentum, and interface capturing advective equations which are given as:

$$\nabla \cdot \boldsymbol{U} = 0 \tag{1}$$

$$\frac{\partial(\rho \boldsymbol{U})}{\partial t} + \nabla \cdot (\rho \boldsymbol{U}\boldsymbol{U}) = -\nabla p + \nabla \cdot \boldsymbol{\tau} + \rho \boldsymbol{g} + \boldsymbol{F}_\sigma \tag{2}$$

$$\frac{\partial \alpha}{\partial t} + \nabla \cdot (\alpha \boldsymbol{U}) - \alpha(\nabla \cdot \boldsymbol{U}) = 0 \tag{3}$$

where ρ is the fluid density, $\boldsymbol{U}$ the fluid velocity vector, $\boldsymbol{\tau}$ the viscous stress tensor, p the pressure, $\boldsymbol{F}_\sigma$ the volumetric surface tension force, $\boldsymbol{g}$ the gravitational acceleration and α the interface capturing function. The function α is used to distinguish between the two fluids of the domain. Note that fluid properties such as density ρ and viscosity μ, as well as the surface tension force vary depending on the scalar field α.

The VOF method utilizes a volume fraction defined as a step function, which is defined in the range [0,1]. Here, the immiscible droplet is defined by cells where $\alpha = 1$, while the water is defined by cells with $\alpha = 0$. The interface is then smeared over the cells where $\alpha \in [0,1]$. The interface capturing advection equation is simplified by using the continuity equation which results in:

$$\frac{\partial \alpha}{\partial t} + \nabla \cdot (\alpha \boldsymbol{U}) = 0 \tag{4}$$

To ensure mass conservation and impose proper boundary conditions, OpenFOAM uses an algebraic counter-gradient transport approach to advect the volume fraction. This results in the addition of a compressive term to the α equation. The advection equation then becomes:

$$\frac{\partial \alpha}{\partial t} + \nabla \cdot (\boldsymbol{U}\alpha) + \nabla \cdot \left(\boldsymbol{U}_c \alpha(1-\alpha)\right) = 0 \tag{5}$$

where $\boldsymbol{U}_c = \boldsymbol{U}_f - \boldsymbol{U}_w$ is the compressive velocity. The subscripts f and w correspond to the Fluorinert™ and water, respectively. The compressive velocity is only taken into account in the region of the Fluorinert™/water interface. A compressive factor c_α is used to increase compression as:

$$\boldsymbol{U}_c = \min(c_\alpha |\boldsymbol{U}|, \max(|\boldsymbol{U}|)) \frac{\nabla \alpha}{|\nabla \alpha|} \tag{6}$$

A compression factor of $c_\alpha = 1$ was used for all computational results presented here. Physical properties are calculated using weighted averages by

$$\rho = \rho_f \alpha + \rho_w (1-\alpha) \tag{7}$$

$$\mu = \mu_f \alpha + \mu_w (1-\alpha) \tag{8}$$

A Continuum Surface Force model (CSF) is used to calculate the volumetric surface tension force and is given as

$$\boldsymbol{F}_\sigma = \sigma \kappa(\alpha) \nabla \alpha \tag{9}$$

where $\kappa(\alpha)$ is the interface curvature, which is calculated based on updated values of α. The magnitude of the interface normal flux at a specific face of the cell defines the curvature, and is given by

$$\kappa = -\nabla \cdot (\boldsymbol{n}_c \cdot \boldsymbol{S}_{face}) \tag{10}$$

where $\boldsymbol{S}_{face}$ is the surface vector of the cell face and $\boldsymbol{n}_c$ is the unit interface normal, which is calculated from the phase fraction field by

$$\boldsymbol{n}_c = \frac{(\nabla \alpha)_{face}}{|(\nabla \alpha)_{face}|} \tag{11}$$

At wall boundaries, a constant contact angle boundary condition is used where the angle is defined as the angle between the interface normal and the unit normal $\boldsymbol{n}_{face}$ at the wall by

$$\boldsymbol{n}_c \cdot \boldsymbol{n}_{face} = cos\theta \tag{12}$$

Aluminum was used to make the engineered fractures in the reported results. Also note that, from experimental measurements it was found that, Fluorinert™ has a contact angle of approximately zero degrees with aluminum, the material used to make engineered fractures .

5.2 Simulation Example

Computational results are compared with experimental images for a flow rate of 0.756 l/min for a smooth fracture with an aperture of 1.6 mm, height of 31.75 mm and length of 152.4 mm. The VOF simulations were performed on a hexahedral mesh, and automatic mesh refinement was used to accurately capture the Fluorinert™ /water interface. The mesh was refined/unrefined at each time step in order to capture the interface. The flow field was first initialized to steady state and a sphere shaped Fluorinert droplet with a diameter of 1.4 mm was placed upstream of the fracture. The droplet and flow field velocities along the fracture (test section) are shown in figure 8 below. It is noted that the Fluorinert™ droplet exhibits little velocity lag initially, but experiences a sudden decrease as it progresses through the fracture. This decrease is due to its interaction with the walls of the fracture. In this particular simulation, the droplet contacts one of the walls from $x/L = 0.4$ onward. This behavior is consistent with experimental observations where large droplets have been seen to decelerate and even stop within the image view.

A comparison of simulated droplet shape and imaged droplet shape as it moves through the fracture is shown below in figure 9. The shapes of the moving droplet are comparable between simulation and experiment indicating that the simulation produces a reasonable representation of the fluid forces acting on the droplet. The side view of the droplet velocity magnitude contour plot also provides a visual description of the droplet adhesion to the fracture wall. It is also noted that the droplet velocity predicted for the midpoint of the test section and onward is very close to the experimentally measured value for the 0.825 l/min flow rate as shown in table 1. This gives additional confidence that this simulation approach is an excellent tool for understanding the flow field.

These simulation results highlight the importance of droplet size, especially when surface factors such as wettability apply. Smaller droplets (which will be considered in follow-on research) are less likely to contact the fracture walls and produce lag behaviors. Additionally, the use of a contrast agent with poor surface wetting properties is also desired to mitigate the lag caused by surface wetting.

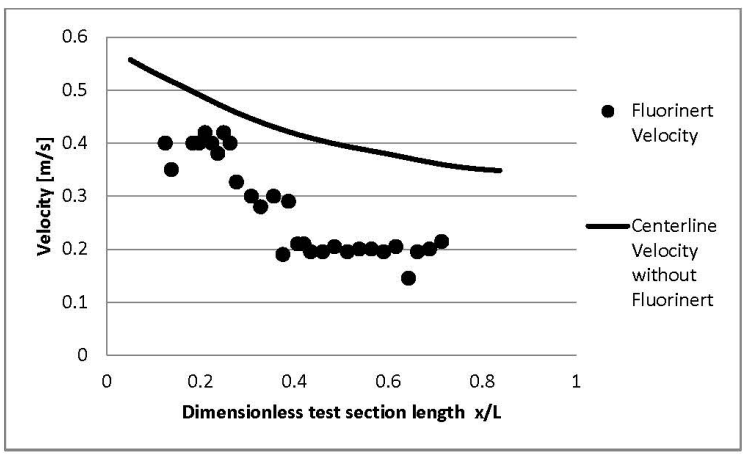

Figure 8: VOF centerline flow velocity and droplet velocity along the length of the fracture

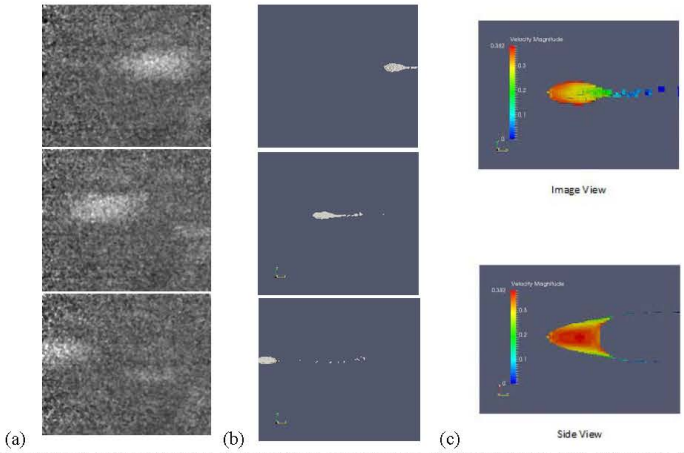

(a) (b) (c)

Figure 9: (a) Captured droplet images, (b) simulated droplet images and (c) image and side views of droplet velocity magnitudes

CONCLUSION

An experimental method for performing particle imaging velocimetry of aqueous flow through a fractured sample within a pressure vessel using neutron radiography has been demonstrated. Multiple contrast agents were explored as candidate tracked objects, but the greatest success to date has come using an immiscible fluid that is less susceptible to dilution effects. Dilution of the contrast agent complicates the tracking of the spatial location of the contrast agent making it difficult or impossible to ascertain the flow field. The immiscible agent that has been utilized, Fluorinert™, is not ideal. Its properties are not well matched to water and it has an extremely high wettability that makes it susceptible to sticking to the fracture walls. The selection of a contrast agent with better matched fluid properties and reduced wettability is needed to improve the performance of the method and will be a future focus of this research. Control of the droplet size introduced into the flow field can mitigate the poor property matching and wettability effects and permit improved correlation of the droplet velocity vector to the fluid velocity field. A method for introducing more controlled droplet size and seeding frequency was described in this work, but the first experimental attempt to use this technique was unable to definitively validate the approach because the acquired radiographs were of poor quality due to the configuration of the neutron instrument at the time.

While continued refinement of this method is needed, results to date indicate that it has the potential to enhance understanding of and quantifying of flow field structure in fractured geological media. A method for simulating droplet behavior using a Navier-Stokes based fluid behavior model was also presented in this work. Such tools are often used to simulate complex scenarios on smaller scales in order to develop reduced-order representations that can be applied to larger scales such as reservoir simulations. The validation of such simulation based approaches in developing reduced-order representations is critical and it is believed that experimental capabilities of the type described in this paper are well suited for this purpose.

ACKNOWLEDGMENT

Research supported by the Geothermal Technologies Office, Office of Energy Efficiency and Renewable Energy, U.S. Department of Energy under contract DE-AC05-00OR22725, Oak Ridge National Laboratory, managed and operated by UT-Battelle, LLC.

Part of this research conducted at ORNL's High Flux Isotope Reactor was sponsored by the Scientific User Facilities Division, Office of Basic Energy Sciences, US Department of Energy.

We also acknowledge the support of the National Institute of Standards and Technology, U. S. Department of Commerce, in providing neutron research facilities used for part of this work.

REFERENCES

Adrian, R.: Particle-Imaging Techniques for Experimental Fluid Mechanics, *Ann. Rev. Fluid Mech.*, **23**, (1991), 261-304.

Babadagli, T., Ren, X., and Develi, K.: Effects of Fractal Surface Roughness and Lithology on Single and Multiphase Flow in a Single Fracture: An Experimental Investigation, *Int. J. of Multiphase Flow,* **68**, (2015), 40-58.

Berkowitz, B.: Characterizing Flow and Transport in Fractured Geological Media: A Review, *Advances in Water Resources,* **25,** (2002), 861-884.

Dijk, P. and Berkowitz, B.: Investigation of Flow in Water-Saturated Rock Fractures Using Nuclear Magnetic Resonance Imaging (NMRI), *Water Resources Research,* **Vol. 35, No. 2,** (1999), 347-360.

Dijk, P. and Berkowitz, B.: Three-Dimensional Flow Measurements in Rock Fractures, *Water Resources Research,* **Vol. 35, No. 12,** (1999), 3955-3959.

Hakami, E. and Larsson, E.: Aperture Measurements and Flow Experiments on a Single Natural Fracture, *Int. J. Rock Mech. Min. Sci. & Geomech. Abstr.*,**Vol. 33, No.4**, (1996), 395-404.

Jacobson, D.L., Hussey, D.S., Baltic, E., LaRock, Arif, J.M., Gagliardo, J.,Owejan, J.P., and Trabold, T.A.: Neutron Radiography And Tomography Facilities At NIST To Analyze In-Situ PEM Fuel Cell Performance", D.L. Jacobson, D.S. Hussey, *8th World Conference on Neutron Radiography*, Gaithersburg,MD, Oct. 16-20 (2006).Klimczak, C., Schultz, R.A., Parashar, R. and Reeves, D.M.: Cubic Law with Aperture-Length Correlation: Implications for Network Scale Fluid Flow, *Hydrogeology Journal,* **18 (4)**, (2010), pp. 851-862.

Neuzil, C.E. and Tracy, J.: Flow Through Fractures, *Water Resources Research*, **Vol. 17, No. 1**, (1981), 191-199.

Polsky, Y., Anovitz, L. M., Bingham, P. and Carmichael, C.: Application of Neutron Imaging to Investigate Flow Through Fractures for EGS, *Proceedings,* 38th Workshop on Geothermal Reservoir Engineering, Stanford University, Stanford, CA (2013).

Qian, J., Chen, Z., Zhan, H., and Guan, H.: Experimental Study of the effect of Rougness and Reynolds Number on Fluid Flow in Rough-Walled Single Fractures: a Check of Local cubic Law, *Hydrological Processes*, **Vol. 25, Iss. 4**, (2011), 614-622.

Rush, T.A., Newell, T.A. and Jacobi, A.M.: An Experimental Study of Flow and Heat Transfer in Sinusoidal Wavy Passages, **Vol. 42, Iss. 9**, (1999), 1541-1553.

Waite, M.E., Ge, S. and Spetzler, H.: A New Conceptual Model for Fluid Flow in Discrete Fractures: An Experimental and Numerical Study, *Journal of Geophysical Research,* **104**, (1999), pp. 13,049 – 13,059.

Witherspoon, P.A., Wang, J.S.Y., Iwai, K. and Gale, J.E.: Validity of Cubic Law for Fluid Flow in a Deformable Rock Fracture, *Water Resources Research,* **Vol. 18, No. 6,** (1980), 1016-1024.